Published in final edited form as:
Biomaterials. 2014 December ; 35(36): 9581–9590. doi:10.1016/j.biomaterials.2014.08.015.

Enhancement of the propagation of human embryonic stem cells by modifications in the gel architecture of PMEDSAH polymer coatings

Xu Qian[a,d], **Luis G. Villa-Diaz**[a,d], **Ramya Kumar**[c,d], **Joerg Lahann**[b,c,d], and **Paul H. Krebsbach**[a,b,d,*]

[a]Department of Biologic and Materials Sciences, School of Dentistry, University of Michigan, Ann Arbor, MI, USA

[b]Department of Biomedical Engineering, University of Michigan, Ann Arbor, MI, USA

[c]Department of Chemical Engineering, University of Michigan, Ann Arbor, MI, USA

[d]Biointerfaces Institute, University of Michigan, Ann Arbor, MI, USA

Abstract

Well-defined culture conditions are essential for realizing the full potential of human embryonic stem cells (hESCs) in regenerative medicine where large numbers of cells are required. Synthetic polymers, such as poly[2-(methacryloyloxy) ethyl dimethyl-(3-sulfopropyl) ammonium hydroxide] (PMEDSAH), offer multiple advantages over mouse embryonic fibroblasts (MEFs) and Matrigel™ for hESC culture and expansion. However, there is limited understanding of the mechanisms by which hESCs are propagated on synthetic polymers coatings. Here, the effects of PMEDSAH gel architecture on hESC self-renewal were determined. By increasing the atom transfer radical polymerization (ATRP) reaction time, the thickness of PMEDSAH was increased and its internal hydrogel architecture was modified, while maintaining its overall chemical structure. A 105 nm thick ATRP PMEDSAH coating showed a significant increase in the expansion rate of hESCs. Theoretical calculations suggested that 20,000 hESCs cultured on this substrate could be expanded up to 4.7×10^9 undifferentiated cells in five weeks. In addition, hESCs grown on ATRP PMEDSAH coatings retained pluripotency and displayed a normal karyotype after long-term culture. These data demonstrate the importance of polymer physical properties in hESC expansion. This and similar modifications of PMEDSAH coatings may be used to obtain large populations of hESCs required for many applications in regenerative medicine.

*Corresponding author: 1011 N. University, Room K, 1030, Ann Arbor, MI 48109-1078, USA. Tel: +1 734 763 5280, Fax: +1 734 763 3453, paulk@umich.edu (P.H. Krebsbach).

Author contributions: X.Q.: conception and design, collection and/or assembly of data, data analysis and interpretation, manuscript writing, and final approval of manuscript; L.G.V-D: collection and/or assembly of data, data analysis and interpretation, and final approval of manuscript; R.K.: collection and/or assembly of data, data analysis and interpretation, manuscript writing, and final approval of manuscript; J.L. conception and design, data interpretation, manuscript writing, and final approval of manuscript; P.H.K.: conception and design, data analysis and interpretation, manuscript writing and final approval of manuscript.

1. Introduction

Because of the capacity to self-renew indefinitely and to differentiate into specialized cell types of all three germ layers and trophectoderm, human embryonic stem cells (hESCs) have become a potential source of cells for regenerative medicine, tissue engineering, disease modeling and drug screening. However, the successful therapeutic application of hESCs and their derivatives is based on the ability to develop clinically compliant strategies for large-scale bioprocessing of therapeutically relevant cells [1–3].

Currently, the large-scale expansion methods for hESCs and induced pluripotent stem cells (iPSCs) are limited by xenogeneic components and poorly defined culture conditions that utilize feeder cells and other animal-based products to support hESC self-renewal [4–6]. To overcome these limitations, the use of human recombinant proteins like laminin isoforms -111, -332, 511, vitronectin, or E-cadherin have been tested for long-term maintenance of hESCs [7–9]. These findings suggest a trend in the evolution of hESC culture from feeder-cell dependence and ill-defined conditions, to feeder-free and defined microenvironments [10]. However, purification of human recombinant proteins is costly and significantly limits their potential for large-scale propagation of hESCs. Likewise, the inclusion of protein-based substrates adds a level of complexity to the study of the mechanisms by which a surface coating supports the pluripotency of hECSs.

Recently, synthetic substrates [11–19] have demonstrated high potential for large-scale expansion of hESCs because they exhibit the following effective features: completely defined chemical composition, stability during storage, reproducibly synthesized, cost-effectiveness, and compatibility with standard sterilization techniques [20]. Among these synthetic substrates is poly[2-(methacryloyloxy) ethyl dimethyl-(3-sulfopropyl) ammonium hydroxide] (PMEDSAH), a fully defined synthetic polymer coating, developed through a surface initiated graft polymerization technique, which has demonstrated effective capacity to support hESC self-renewal and expansion in long-term culture [14, 21].

Recent evidence suggests that physico-chemical properties, such as hydrophilicity [14], surface roughness [22] and stiffness [23, 24] can impact the capability of synthetic substrates to support hESC growth [10]. However, the mechanisms by which PMEDSAH and other synthetic substrates maintain self-renewal of hESCs are not yet clearly understood. Therefore, we hypothesized that the physical properties of PMEDSAH coatings, as determined by the interfacial architecture of the zwitterionic surface layer, can influence the self-renewal of hESCs. In this study, PMEDSAH films with different thicknesses were prepared on tissue culture polystyrene using a combination of chemical vapor deposition polymerization [24] and atom transfer radical polymerization (ATRP) [25]. The impact of gel architecture on hESC self-renewal was then tested on PMEDSAH polymer coatings over a range of thicknesses.

2. Materials and methods

2.1. Synthetic surface preparation and characterization

2.1.1. UVO-initiated free radical polymerization—UVO-initiated free radical polymerization was carried out in a fume hood with connections for argon and vacuum. A 500 mL reaction vessel was degassed by vacuum for 60 minutes. While the reaction vessel was being evacuated, a monomer solution consisting of 0.25 M MEDSAH (Sigma Aldrich) was dissolved in a mixture of deionized water and ethanol (4:1, v/v). The solution was degassed for 40 minutes using an argon purge. Once the reaction vessel and solvent were degassed, the monomer solution was transferred to a reaction vessel and heated to 68–70°C. While the reaction vessel was being heated, TCPS dishes (BD Biosciences) were activated by UV ozone treatment (Jetlight Inc.) for 40 minutes to create initiation sites on the surface. Samples without functionalization that consisted of poly-p-xylylene coated silicon wafers and gold wafers were also added to the cell culture dishes to enable thickness and contact angle measurement. After activation, the dishes were transferred to a reaction vessel and the temperature was raised to 76–80°C. Surface-initiated polymerization occurred over a 2.5 hr time period under argon atmosphere at 76–80°C. Once the process was complete, TCPS plates and control samples were removed from the reaction vessel and were rinsed in a 1% saline (w/v) solution at 50 °C.

2.1.2. CVD and Ellipsometry—The initiator used for ATRP was synthesized through chemical vapor deposition (CVD) polymerization of 40 mg of [2.2]paracyclophane-4-methyl-2-bromoisobutyrate precursor, which was loaded into the sublimation zone. Sublimation occurred at 120°C, followed by pyrolysis at 540–550°C, after which a thin film of poly[(p-xylylene-4-methyl-2-bromoisobutyrate)-co-(p-xylylene)] was coated on the target substrates. The tissue culture polystyrene (TCPS) plates as well as surrogates (gold and silicon wafers) were placed on a rotating stage in the deposition chamber and were maintained at 15°C during CVD polymerization. Ellipsometry was performed on the silicon wafers to measure thickness of the initiator coating before and after the ATRP. Film thickness was assessed with a multi-wavelength imaging null-ellipsometer (EP3 Nanofilm, Germany). Fixed values of the real (n=1.58) and imaginary (k=0) refractive index of the polymer coatings and the ellipsometric delta and psi were used to determine film thickness. After the reaction was completed, the thickness of PMEDSAH coating was calculated by subtracting the initial thickness from the post-reaction thickness.

2.1.3. Atom transfer radical polymerization—Poly[2-(methacryloyloxy)ethyl dimethyl-(3-sulfopropyl)ammonium hydroxide] (PMEDSAH) (Monomer Polymer Dajac Labs, Trevose, PA) was polymerized using an ATRP procedure. Initiator coated substrates were prepared according to the CVD process described above. Initiator-coated samples and TCPS were placed in a glove bag and degassed using 3 cycles of vacuum-argon purge and left at room temperature under argon. A 4:1(v/v) mixture of methanol and water was degassed by three cycles of freeze-pump-thaw. Approximately 20% of the degassed solvent was transferred to a degassed flask. The monomer was then dissolved in the main flask and the copper/ligand mixture was dissolved in the second flask. After 10 minutes the catalyst mixture was added to the monomer solution and mixed thoroughly at room temperature. The

polymerization solution was finally transferred to the glove bag and distributed among the TCPS and the surrogates, so that each substrate was submerged completely. The ATRP reaction was allowed to proceed for 1, 12, and 24 hours under argon atmosphere. After ATRP, surrogates and TCPS plates were rinsed with 1% sodium chloride solution and deionized water and dried. Residual copper was removed from the ATRP-modified surfaces by washing alternately with 5 mM ethylenedimaine tetracetic acid sodium salt (EDTA) and 5mM calcium chloride solutions and finally with deionized water.

2.1.4. Contact angle—Static contact angles of deionized water were measured using a contact angle goniometer (Ramé-Hart 200-F1 goniometer). Measurements were taken at three different locations and averaged.

2.1.5. Streaming potential measurement—Polymer coatings were prepared directly on polystyrene slides to measure surface charge. An electrokinetic analyser SurPASS (Anton Paar GmBH) was used in clamping cell mode to acquire zeta potential values of the samples across a 3–10 pH range. Two titrations were performed for each sample, one proceeding from the neutral to the acidic range and another from the neutral to the basic range. 0.1 M hydrochloric acid and 0.1M sodium hydroxide were used as titrants. 0.001 M potassium chloride was used as the electrolyte. pH changes were performed using an automated titration unit with pH being altered in steps of 0.3 with continuous stirring of the electrolyte solution. Streaming current was measured using Ag/AgCl electrodes and the helmohltz smoluchwski equation was used to compute the zeta potentials. Flow rates of 50–70 ml/minute were used at a pressure of 400 mbar and a gap of 100 microns between the sample and the polypropylene reference standard. Samples were rinsed for 3 minutes in between measurements at different pH points.

2.1.6. Atomic force microscopy (AFM)—The surface roughness of the PMEDSAH coatings was quantified via atomic force microscopy (AFM) using a Dimension Icon (Bruker, Madison, WI). Measurements were taken in tapping mode at room temperature in air using NSC15 cantilevers (MikroMasch, San Jose, CA) with resonant frequency and spring constants of 20–75 N/m and 265–400 kHz, respectively as probe tips. Measurements were taken at 1 Hz scan rate over a 2×2 micron area. Roughness values in the form of root mean square roughness (R_a) were acquired through a statistical analysis performed by the AFM software (NanoScope Analysis) by averaging over the scanned region. Three values were acquired for each sample and averaged.

2.2. Preparation of Matrigel-coated substrates

Matrigel (BD BioSciences) was diluted to a concentration of 0.1mg/ml in cold Dulbecco's modified Eagle's medium/F12 (DMEM/F12; GIBCO) and then applied to tissue culture polystyrene (TCPS) dishes (35 mm; BD Falcon). The coating was allowed to polymerize during 2 h incubation at room temperature. Before plating cells, excess Matrigel-DMEM/F12 solution was aspirated and the dishes were washed with sterilized Dulbecco's phosphate buffered saline (D-PBS).

2.3. hESC culture

hESCs (H9 and H1, WiCell Research Institute, Madison, WI; CHB10, Children's Hospital Corporation, Boston, MA) were cultured on PMEDSAH with human-cell-conditioned medium (HCCM, Global Stem) supplemented with 5ng/mL of human recombinant basic fibroblast growth factor (bFGF; Invitrogen[trade;]). Differentiated cells were mechanically removed using a sterile pulled-glass pipet under a stereomicroscope (LeicaMZ9.5, Leica Microsystems Inc., Buffalo Grove, IL). Undifferentiated colonies were cut and collected as small cell clusters into a 1.5 mL centrifuge tube. After centrifugation and brief washing with PBS, cells were treated with 0.5 mL 0.25% Trypsin-EDTA (GIBCO) at 37°C. The trypsinization was terminated by the addition of 1ml HCCM and brief centrifugation. The cell pellet was dispersed in HCCM supplemented with 5ng/mL bFGF and 10 μM of ROCK inhibitor (Sigma) [26] and passed through a 40 μm nylon mesh cell strainer (BD Biosciences, Bedford, MA) to remove large cell aggregates. Single hESCs were counted and 20,000 cells (2000 cells/cm^2) were plated on Matrigel, PMEDSAH and three types of ATRP PMEDSAH (25nm, 105nm and 176nm thick) coated-dishes and cultured for 7 days. The culture medium was replaced every other day. Single hESCs were passaged once a week for 5 consecutive weeks using the same method without removing differentiated colonies before passage.

2.4. Alkaline phosphatase assay

An Alkaline Phosphatase Detection Kit (Millipore) was used for phenotypic assessment of hESC. Briefly, on day 7, cells were fixed with 4% paraformaldehyde in PBS for 1–2 minutes, then rinsed and incubated in staining solution in the dark at room temperature for 15 minutes. Cells were rinsed and covered with 1x PBS to prevent drying prior to quantitative analysis. Undifferentiated colonies were identified by specific alkaline phosphatase staining.

2.5. Quantitative analysis of undifferentiated colony formation and the total cell number

ImageJ software (http://rsb.nih.gov/ij) was used to count the number and area of undifferentiated colonies stained by alkaline phosphatase. The total number of cells grown on each dish was counted with a hemocytometer at the time of passage during the 5 consecutive weekly passages. A theoretical yield of total cell number of hESCs obtained on different substrates was calculated assuming that all cells would be passaged each week instead of the only 20,000 single cells that were done. The theoretical yield of cells was determined with the formula $CN_{(n+1)} = CN_n \times TN_{(n+1)}/20000$, in which *CN* is the calculated total cell number, *TN* is the total cell number and *n* is the passage number.

2.6. Flow cytometry analysis

hESCs cultured on different substrates from week 1 to 5 were washed with PBS and harvest by incubation in 0.25% trypsin-EDTA (GIBCO). The trypsinization was terminated by adding1ml HCCM and the cells were incubated first with human IgG to block un-specific binding and then with human/mouse SSEA-4 PE-conjugated antibody (R&D systems) and analyzed by flow cytometry. Analysis was carried out with MoFloR® Astrios™ (Beckman Coulter) using standard procedures. Background fluorescence and autofluorescence were

determined using cells incubated with Mouse IgG1 phycoerythrin isotype Control (R&D systems).

2.7. Immunofluorescence staining

Cells grown on different substrates were fixed in 4% paraformaldehyde for 30 min at room temperature and then permeabilized with 0.1% Triton X-100 for 10 min. Primary antibodies raised against SSEA-4 (Santa Cruz Biotechnology), OCT3/4 (Santa Cruz Biotechnology), SOX2 (Millipore), TRA-1-60 (Santa Cruz Biotechnology), TRA-1-81 (Millipore), and NANOG (Abcam) were diluted in 1% normal serum and incubated overnight at 4°C and detected with respective secondary antibodies. Sample images were captured using a Nikon TE2000-S inverted microscope with a Nikon DS-Ri1 camera.

2.8. RNA isolation and quantitative RT-PCR

Cells grown on different substrates were manually scraped from dishes and pelleted by centrifugation. RNA was isolated and purified using the RNA easy Mini-Kit (Qiagen) following the manufacturer's protocol. RNA quality and concentration was checked with a Synergy NEO HTS Multi-Mode Microplate Reader (BioTek Instruments, Winooski, VT).

Reverse transcription from 1 μg of total RNA into cDNA was done using SuperScript™ III First-Strand Synthesis SuperMix (Invitrogen™). Quantitative PCR was performed using TaqMan probes (Applied Biosystems) and TaqMan Universal PCR Master Mix (Applied Biosystems) on 7900 HT Fast Real Time PCR system (Applied Biosystems). Gene expression data was normalized to the expression levels of GAPDH, and calculated using the delta-delta *cT* expression level.

2.9. Analysis of hESC pluripotency

At passage 5, pluripotency of hESCs was tested by embryoid body (EB) formation and directed cell-lineage differentiation. EB formation was achieved by hESC clusters cultured in suspension in DMEM (Life Technologies) supplemented with 10% FBS for 10 days to promote differentiation. Directed cell-lineage differentiation was performed on Matrigel using the following protocols [27]. hESCs were induced to differentiate in chemically defined medium (CDM) base consisting of DMEM/F12 (Invitrogen) supplemented with 1X N2 (Invitrogen), 1X B27 (Invitrogen), 0.11 mM 2-mercaptoethanol, 1 mM nonessential amino acids, 2 mM L-glutamine, and 0.5 mg/ml BSA (fraction V; Sigma Aldrich). To induce definitive endoderm (pancreatic differentiation) 100 ng/ml human recombinant activin A (STEMGENT) was added to CDM and cells were cultured in this condition for 6 days, followed by culture in CDM without activin A for an additional 9 days. For mesoderm (cardiomyocyte differentiation) cells were cultured in CDM supplemented with 50 ng/ml human recombinant BMP4 (STEMGENT) and 50 ng/ml human recombinant activin A (STEMGENT) for 4 days, then further cultured in CDM with no activin A and BMP4 for another 10 days. For ectoderm (neuronal differentiation), 100 ng/ml human recombinant Noggin (STEMGENT) was added to the CDM and cells were cultured in this condition for 8 days.

2.10. Cytogenetic evaluation

After 5 weeks of cell culture, standard G-band analysis on at least 20 cells was performed on cells cultured on 105nm ATRP PMEDSAH by Cell Line Genetics (Madison, WI) using standard protocols.

2.11. Data analysis

Three independent replicates for each experiment were performed. Two data sets were compared using unpaired student t-test function in Excel (Microsoft, Seattle, WA) to calculate p values. Multiple data sets were compared using one way ANOVA analysis followed by the Tukey's post hoc test to calculate p values. Levels of statistical significance were set at $p < 0.05$.

3. Results

3.1. Differences in properties of PMEDSAH coatings

PMEDSAH polymer coatings were fabricated using two different surface-initiated polymerization procedures: UVO-initiated free radical polymerization (UVO-grafting) [21] and atom transfer radical polymerization (ATRP) conducted at three different reaction times. Physicochemical comparison between these four coatings was based on film thickness, wettability, surface roughness and zeta potential measurements (Fig. 1). The thickness of films prepared through UVO-grafting was of 25 ± 6.5 nm. In contrast, ATRP-prepared coatings displayed a gradual augmentation in film thickness with increasing reaction time: 25 ± 3 nm in a 1 hour-reaction; 105 ± 8 nm in a 12 hour-reaction; and up to 176 ± 18.2 nm in a 24 hour reaction (Fig. 1A). The contact angle of UVO-grafted PMEDSAH was 16.6 ± 1.6°, while ATRP film thicknesses that ranged between 25 nm and 176 nm demonstrated an increase in the contact angle from 21.9 ± 9.4° to 75.3 ± 4° (Fig. 1B). In several studies, engineering roughness into soft cell culture substrates in the form of nano-grooves and pillars has been shown to play a role in mediating cell adhesion [28]. Thus, the roughness of the four coatings was quantified with a topographical examination using atomic force microscopy. Differences in roughness, as measured by root-mean-square roughness values, were not statistically significant among the four coatings (Fig. 1A). The zeta potential of grafted PMEDSAH was less negative than ATRP coatings. In addition, the 25 nm and 176 nm thick PMEDSAH coatings exhibited more negative charge than the 105nm thick coating in the neutral range of pH values. The isoelectric point of the 105 nm thick ATRP coating shifted slightly to the right from that of the other two coatings, indicating that it was less negative in terms of charge (Fig. 1C).

3.2. Propagation of undifferentiated hESC colonies

Alkaline phosphatase activity was used to identify undifferentiated hESC colonies. When CBH10 hESCs were initially cultured as single cells on ATRP PMEDSAH with a surface thickness of 105 nm, the number of undifferentiated colonies was similar to that of the Matrigel control group (Fig. 2A–B). However, compared to the other experimental groups, a significantly higher number of colonies were detected on the 105 nm thickness group. No significant differences in colony surface area were observed among experimental groups (Fig. 2A–B). Similar results were obtained with the H9 hESC line, which limits the

possibility of a hESC line-specific effect (Supplementary Fig. 1). Taken together, these results indicated that the gel architecture of PMEDSAH coatings influenced hESC colony formation.

3.3. hESC expansion

To quantify the impact of gel architecture on long-term expansion of hESCs, a consistent number (20,000) of hESCs cultured initially as single cells on Matrigel, PMEDSAH and ATRP PMEDSAH (25 nm, 105 nm, 176 nm) were passaged weekly for five consecutive weeks. Prior to each passage to newly coated dishes, the total cell number was quantified and flow cytometry was performed on a subset of cells to evaluate the expression of SSEA-4, a hESC marker (Supplementary Fig. 2). The percentage of SSEA-4 positive cells ranged from 96.65% to 99.95% and was not statistically ($p>0.05$) different among the different substrates and passages. However, the total number of cells that adhered to Matrigel decreased after each passage and cells on Matrigel did not survive after four consecutive passages. In contrast, single hESCs cultured on ATRP PMEDSAH and grafted PMEDSAH continued to thrive with each passage. Growth of hESCs was particularly robust on the ATRP PMEDSAH with a 105 nm surface thickness that supported a significantly ($p<0.05$) higher total cell number than all other experimental groups (Fig. 2C).

The hypothetical yield of total hESCs achieved after five passages on each substrate was calculated assuming that all cells obtained at each passage were sub-cultured, instead of the 20,000 cells that were actually propagated. The theoretical yield of cells was determined using the formula $CN_{(n+1)} = CN_n \times TN_{(n+1)}/20000$. In this formula, CN was the calculated total cell number, TN was the total cell number in the determined week and n represented the culture week. Using this formula, it was estimated that on the 105nm thick-ATRP PMEDSAH, the expansion of 20,000 cells over a period of five weeks would yield up to 4.7×10^9 undifferentiated stem cells. This level of hESC expansion on the 105 nm thick-ATRP PMEDSAH was 33.6-, 1.6- and 12.7-fold greater than the theoretical yield calculated when cultured on grafted PMEDSAH, 25 nm and 176 nm thickness-ATRP PMEDSAH, respectively (Table 1). These calculated total cell numbers strongly demonstrated that modifying the gel architecture significantly facilitated the expansion of hESCs.

3.4. hESC pluripotency and genomic stability

Quantitative RT-PCR analysis of cells after five passages demonstrated that RNA expression levels of hESC markers *OCT4, SOX2, KLF4* and *NANOG* were similar among hESCs cultured on grafted PMEDSAH and ATRP PMEDSAH (25nm, 105nm, 176nm; Fig. 3A). Immunofluorescent staining of OCT4 and SSEA-4 in hESCs was also strong when cultured on both grafted PMEDSAH and ATRP PMEDSAH (25 nm, 105 nm and 176 nm) coatings (Fig. 3B). Because 105 nm ATRP PMEDSAH demonstrated a stronger capacity to support hESC self-renewal and expansion, an additional hESC line was also cultured on 105 nm ATRP PMEDSAH during the same period of time. In addition to OCT4 and SSEA-4, primary antibodies to SOX2, NANOG, TRA-1-60 and TRA-1-81 were used for immunofluorescence staining of H1 hESCs and all stem cell markers were strongly expressed (Fig. 3C).

The pluripotency of hESCs cultured on the 105 nm thick-ATRP PMEDSAH was determined by embryoid body (EB) formation and directed cell-lineage differentiation after five passages. Clusters of hESC cultured on 105 nm thick-ATRP PMEDSAH formed EBs when cultured in suspension and expressed genes representing endoderm, mesoderm and ectoderm (Table 2). Furthermore, specific cell-lineage differentiation was successfully directed *in vitro* with chemically defined conditions, as demonstrated by a significant increase in expression of representative genes for each germ layer: *AFP FOXA2, PDX1* and *SOX17 for endoderm; HESX1, NKX2-5* and *TNN13* for mesoderm; and *NES, NEUROD1, PAX6* and *SOX1* for ectoderm (Fig. 4). These results demonstrated that ATRP PMEDSAH with a 105 nm surface thickness supported the pluripotency of hESCs.

Because chromosomal changes may occur during long-term culture of hESCs [29], the genetic stability of cells cultured on 105 nm thick-ATRP PMEDSAH was evaluated by standard G-band analysis after five passages. The results demonstrated a normal human male karyotype for the H1 cell line (Fig. 3D).

4. Discussion

The evolution of hESC culture from feeder-cell dependence and non-defined conditions to feeder-free and defined microenvironments has been enabled by the development of new culture materials. Because of its strong capacity to support hESC and induced pluripotent stem cell (iPSC) growth with chemically-defined and xenogeneic-free medium, the PMEDSAH-coating has the potential to serve as a substrate to generate high numbers of clinical grade pluripotent stem cells [10]. Thus, the elucidation of mechanisms by which PMEDSAH is able to support hESC self-renewal, pluripotency and long-term propagation will not only advance our knowledge of pluripotent stem cell biology, but also increase the effectiveness of hESC and iPSC expansion on defined conditions for potential human applications.

Because Matrigel is the most commonly used feeder-free substrate for hESC culture, it was used as a control in our experiments. We found that the number of hESCs grown on Matrigel decreased after each passage, which may be due to the poor survival of hESCs on Matrigel after cell dissociation [26, 30]. In contrast, both grafted and ATRP PMEDSAH supported hESC expansion during the five-week expansion period. In particular, the ATRP PMEDSAH with a 105 nm surface thickness led to significantly higher total cell numbers compared to all other experimental groups (Table I). In addition, hESCs retained their pluripotency and a normal karyotype after multiple passages during culture, which indicates that hESCs maintained their unique characteristics and genetic stability. These findings are well aligned with the long-term goal of large-scale production of clinical grade hESCs.

The different surface preparations tested in this study affected the gel architecture of the substrates. The UVO-grafted PMEDSAH surface had thin, poly-dispersed and unassociated polymer brushes. Whereas the ATRP process was capable of producing thick and mono-dispersed polymer brushes [31, 32]. Moreover, the gel architectures were also different among the three ATRP surfaces due to differences in the ATRP reaction time. These data suggest that the gel architecture of the 105 nm thick ATRP coating best supported hESC

growth, supporting the hypothesis that gel architecture of the zwitterionic surface layer is capable of influencing the culture and expansion of hESCs.

The thickness of PMEDSAH produced using a 1-hour ATRP reaction time was nearly equal to that of the UVO-grafted surface (Fig. 1). However, the former was capable of expanding the stem cell population at a higher rate than the latter. Interestingly, the 176 nm thick coating exhibited a lower capacity for hESC expansion than both the thinnest coating (25 nm) and the best-performing PMEDSAH surface for hESC expansion (105 nm). The molecular weight of the UVO-grafted films could not be precisely controlled due to the kinetics of conventional free radical polymerization, where the radical lifetime is short and the termination step is rapid [33]. However, the molecular weight of ATRP films was controlled and augmented as the film thickness increased by longer ATRP reactions. Therefore, the observation that 105 nm thick ATRP films supported hESC self-renewal better than the other ATRP groups with reduced or increased thickness, suggests that an optimal range of molecular weight for synthetic polymer coatings exists for the support hESC self-renewal. This finding is consistent with a recent study in which polymer molecular weight influenced hESC growth in a non-monotonic manner [18]. Another study comparing substrates with different chemical structures demonstrated that hydrophobic materials are less permissive for hESC adhesion [14]. Here, however, we investigated the effects of hydrophilicity on hESC behavior using PMEDSAH surfaces with identical chemical compositions with different degrees of wettability. The UVO- grafted and the 25 nm ATRP-PMEDSAH, which have a contact angle of 16.6° and 21.9°, respectively, were the most hydrophilic surfaces tested. The 176 nm thick ATRP coating, with a contact angle of 75.3°, was the least hydrophilic of all PMEDSAH surfaces tested. However, all three surface coatings demonstrated lower hESC expansion rates compared to the 105 nm thick ATRP-PMEDSAH coating, which had a contact angle of 43.7°. Thus, modifying the PMEDSAH surface to a moderate hydrophilicity led to better support of hESC growth than surfaces at the extremes of contact angle.

The hydrophilicity of UVO-grafted PMEDSAH is attributed to water affinity of the anionic sulphonate and cationic quaternary ammonium present in their side chains. The tendency of these functional groups to be hydrated leads to water penetration, swelling of the polymer brush and a lower contact angle. For film thicknesses between 25 nm and 176 nm, the contact angle increased from 21.9° to 75.3° (Fig. 1B). This transition from hydrophilic to hydrophobic behavior of PMEDSAH was first explained in terms of whether inter-chain associations dominate the hydration behavior of the polymer brush [34]. Differences in wettability between UVO-grafted and ATRP polymer coatings can be attributed to the effect of grafting density and polymer chain length on the balance of inter- and intra-polymer chain associations [35].

Because neither grafting density nor molecular weight distribution can be precisely controlled [36] in UVO-grafted films, the resulting polymer brush is likely to be thin, poly-dispersed and unassociated. In the unassociated state, ionic attractions between the sulphonate and the ammonium groups in the side chains are not dominant, allowing the polymer to be fully hydrated, resulting in a low contact angle [37]. In contrast, ATRP coatings have a controllable and high grafting density that results in greater proximity of

polymer chains and increased opportunities for short-range ionic interactions. The 25 nm films would exhibit only a slight degree of association behavior, as they do not have a sufficient number of ion-pairs and are therefore hydrophilic. The 105 nm and 176 nm coatings, being of higher molecular weight, have a greater number of ion pairs and are able to form stronger intermolecular associations that lead to dehydration and collapse of the brush. This ion-ion pairing prevents complete hydration of the ionic groups and is effective in sealing out water from the polymer coating. As the PMEDSAH polymer grows in length, more ion pairs are created, increasing the strength of the association, extent of water exclusion and contact angle [34].

In the absence of systematic intermolecular associations, the UVO-grafted PMEDSAH brush remains fully hydrated [37]. It was initially believed that water molecules in the polymer brush could reduce the zeta potential through charge screening. Thus, the higher isoelectric point of UVO-grafted PMEDSAH within the ATRP films was attributed to the lack of ion-pairing effects between polymer side chains. In the ATRP coated PMEDSAH films, the 25 nm and 176 nm thick ATRP-PMEDSAH coatings exhibited more cumulative negative charge than the 105 nm thick coating in the neutral range of pH values. The isoelectric point of the 105 nm thick ATRP coating was shifted to the right of the other two coatings, indicating that it was less negative in charge (Fig. 1C). Since even the hydrophilic 25 nm coating had a highly negative surface charge, differences in surface charge among the ATRP coatings could not be attributed to the level of hydration. The coatings with the highest and lowest degrees of ion-pairing (176 and 25 nm, respectively) were similar in their surface charge with their zeta potential plots overlapping in the neutral region. For reasons not yet fully understood, the 105 nm PMEDSAH coating had the least negative surface charge among the three ATRP coatings and this may render this surface as more favorable for cell adhesion.

It has been shown that surfaces with a roughness of Rq = 1 nm, which are categorized as smooth, support hESCs growth better than nano-rough surfaces with a Rq of 75–150 nm [22]. Our analyses of substrate roughness on all four surfaces showed a Ra lower than 2 nm and had no statistical differences among them, which suggested that all these surfaces could be considered as smooth surfaces. It has also been shown that an optimum range of surface charge is associated with maximal cell adhesion to metallic biomaterial surfaces [38]. In our study, it was also observed that an optimum range of surface charge of PMEDSAH supports hESC expansion. The 105 thick-ATRP PMEDSAH films were more favorable for hESC expansion compared to the UVO-grafted films with a lower negative charge and to the 25 nm and 176 nm thick ATRP PMEDSAH films that exhibited a more negative charge. The more negatively charged 25 nm and 176 nm ATRP films may generate stronger repelling forces to cells, as cell membrane potential is typically negative, which may result in an adverse effect on hESC adhesion. However, this would not explain the lower cell expansion observed on UVO-grafted surfaces with the less negative charge. Thus, it is possible that hESCs prefer an optimum range of repelling forces. Alternatively, the UVO-grafted surfaces had unique gel architecture with polydispersed and unassociated polymer brushes compared to the well-uniformed ATRP surfaces. If this were true, then the surface charge may not be the key factor leading to the differences of hESC expansion between UVO-grafted and ATRP PMEDSAH.

Taken together, the observed trend in hESC expansion (105 nm thick PMEDSAH > 25 nm thick PMEDSAH > 176 nm thick PMEDSAH > UVO-grafted PMEDSAH) could not be attributed alone to a single physical property of the substrates studied here. Comparing thickness and contact angle helped establish that differences in gel architecture between coatings existed. Balance between ion-pairing driven inter-molecular association and hydration behaviors of PMEDSAH brushes may dictated the gel architecture adopted in each substrate. Thus, the data suggest that the 105 nm thick ATRP PMEDSAH coating possesses the optimal gel architecture for hESC expansion with its intermediate thickness, hydrophilicity, surface charge, and a moderate degree of inter-chain association. In addition to significantly higher efficiency in hESC expansion during long-term culture, the 105 nm ATRP-PMEDSAH has the following advantages compared to Matrigel: defined molecular composition, more stably on long-term storage minimal lot-to-lot variability, ease of preparation and compatible with standard sterilization techniques. All of these feature make the 105 nm thick ATRP PMEDSAH a very promising substrate to obtain scalable populations of clinical grade hESCs. This could be accomplished by reducing the cell expansion time, production cost, as well as possible contamination and population drift under current culture conditions.

5. Conclusion

Our results revealed differences in gel architecture between UVO-grafted PMEDSAH and in among ATRP-PMEDSAH substrates that point towards alterations in the balance of inter-molecule associations between polymer chains. This in turn influences the interfacial properties of the substrate and exercises a profound effect on the culture and expansion of hESCs. While all four coatings were able to maintain their pluripotency over long-term culture, significant differences in cell expansion were observed. The 105 nm thick ATRP-based coating was found to perform significantly better than the other three substrates. In conclusion, the physical properties influenced the ability of PMEDSAH to support hESC expansion. The newly developed 105 nm thick ATRP-PMEDSAH described here may be effective in the scalable production of hESCs for application in regenerative medicine.

Supplementary Material

Refer to Web version on PubMed Central for supplementary material.

Acknowledgments

The authors thank Dr. Aftin Ross and Gowthamy Venkidasubramonian for their assistance to prepare the PMEDSAH plates, and the National Institutes of Health (R01DE016530-08 to PHK) for support.

References

1. McCall MD, Toso C, Baetge EE, Shapiro AMJ. Are stem cells a cure for diabetes? Clin Sci. 2010; 118:87–97. [PubMed: 19807695]
2. Dominguez-Bendala J, Inverardi L, Ricordi C. Stem cell-derived islet cells for transplantation. Curr Opin Organ Tran. 2011; 16:76–82.

3. Laflamme MA, Chen KY, Naumova AV, Muskheli V, Fugate JA, Dupras SK, et al. Cardiomyocytes derived from human embryonic stem cells in pro-survival factors enhance function of infarcted rat hearts. Nat Biotechnol. 2007; 25:1015–24. [PubMed: 17721512]
4. Thomson JA, Itskovitz-Eldor J, Shapiro SS, Waknitz MA, Swiergiel JJ, Marshall VS, et al. Embryonic stem cell lines derived from human blastocysts. Science. 1998; 282:1145–7. [PubMed: 9804556]
5. Richards M, Tan S, Fong CY, Biswas A, Chan WK, Bongso A. Comparative evaluation of various human feeders for prolonged undifferentiated growth of human embryonic stem cells. Stem Cells. 2003; 21:546–56. [PubMed: 12968109]
6. Xu C, Inokuma MS, Denham J, Golds K, Kundu P, Gold JD, et al. Feeder-free growth of undifferentiated human embryonic stem cells. Nat Biotechnol. 2001; 19:971–4. [PubMed: 11581665]
7. Braam SR, Zeinstra L, Litjens S, Ward-van Oostwaard D, van den Brink S, van Laake L, et al. Recombinant vitronectin is a functionally defined substrate that supports human embryonic stem cell self-renewal via alphavbeta5 integrin. Stem Cells. 2008; 26:2257–65. [PubMed: 18599809]
8. Miyazaki T, Futaki S, Hasegawa K, Kawasaki M, Sanzen N, Hayashi M, et al. Recombinant human laminin isoforms can support the undifferentiated growth of human embryonic stem cells. Biochem Biophys Res Commun. 2008; 375:27–32. [PubMed: 18675790]
9. Nagaoka M, Si-Tayeb K, Akaike T, Duncan S. Culture of human pluripotent stem cells using completely defined conditions on a recombinant E-cadherin substratum. BMC Dev Biol. 2010; 10:60. [PubMed: 20525219]
10. Villa-Diaz LG, Ross AM, Lahann J, Krebsbach PH. Concise Review: The evolution of human pluripotent stem cell culture: fom feeder cells to synthetic coatings. Stem Cells. 2013; 31:1–7. [PubMed: 23081828]
11. Derda R, Li L, Orner BP, Lewis RL, Thomson JA, Kiessling LL. Defined substrates for human embryonic stem cell growth identified from surface arrays. ACS Chem Biol. 2007; 2:347–55. [PubMed: 17480050]
12. Klim JR, Li L, Wrighton PJ, Piekarczyk MS, Kiessling LL. A defined glycosaminoglycan-binding substratum for human pluripotent stem cells. Nat Methods. 2010; 7:989–94. [PubMed: 21076418]
13. Kolhar P, Kotamraju VR, Hikita ST, Clegg DO, Ruoslahti E. Synthetic surfaces for human embryonic stem cell culture. J Biotechnol. 2010; 146:143–6. [PubMed: 20132848]
14. Villa-Diaz LG, Nandivada H, Ding J, Nogueira-de-Souza NC, Krebsbach PH, O'Shea KS, et al. Synthetic polymer coatings for long-term growth of human embryonic stem cells. Nat Biotechnol. 2010; 28:581–3. [PubMed: 20512122]
15. Mei Y, Saha K, Bogatyrev SR, Yang J, Hook AL, Kalcioglu ZI, et al. Combinatorial development of biomaterials for clonal growth of human pluripotent stem cells. Nat Mater. 2010; 9:768–78. [PubMed: 20729850]
16. Irwin EF, Gupta R, Dashti DC, Healy KE. Engineered polymer-media interfaces for the long-term self-renewal of human embryonic stem cells. Biomaterials. 2011; 32:6912–9. [PubMed: 21774983]
17. Li Y, Chuang E, Rodriguez R, Firpo M, Healy K. Hydrogels as artificial matrices for human embryonic stem cell self-renewal. J Biomedical Mater Res A. 2006; 79:1–5.
18. Brafman DA, Chang CW, Fernandez A, Willert K, Varghese S, Chien S. Long-term human pluripotent stem cell self-renewal on synthetic polymer surfaces. Biomaterials. 2010; 31:9135–44. [PubMed: 20817292]
19. Melkoumian Z, Weber JL, Weber DM, Fadeev AG, Zhou Y, Dolley-Sonneville P, et al. Synthetic peptide-acrylate surfaces for long-term self-renewal and cardiomyocyte differentiation of human embryonic stem cells. Nat Biotechnol. 2010; 28:606–10. [PubMed: 20512120]
20. Qian X, Villa-Diaz LG, Krebsbach PH. Advances in culture and manipulation of human pluripotent stem cells. J Dent Res. 2013; 92:956–62. [PubMed: 23934156]
21. Nandivada H, Villa-Diaz LG, O'Shea KS, Smith GD, Krebsbach PH, Lahann J. Fabrication of synthetic polymer coatings and their use in feeder-free culture of human embryonic stem cells. Nature Protocols. 2011; 6:1037–43.

22. Chen W, Villa-Diaz LG, Sun Y, Weng S, Kim JK, Lam RH, et al. Nanotopography influences adhesion, spreading, and self-renewal of human embryonic stem cells. ACS Nano. 2012; 6:4094–103. [PubMed: 22486594]
23. Sun Y, Villa-Diaz LG, Lam RH, Chen W, Krebsbach PH, Fu J. Mechanics regulates fate decisions of human embryonic stem cells. PLoS One. 2012; 7:e37178. [PubMed: 22615930]
24. Jiang XW, Chen HY, Galvan G, Yoshida M, Lahann J. Vapor-based initiator coatings for atom transfer radical polymerization. Adv Funct Mater. 2008; 18:27–35.
25. Wang J, Matyjaszewski K. Controlled/“living” radical polymerization. halogen atom transfer radical polymerization promoted by a Cu(I)/Cu(II) redox process. Macromolecules. 1995; 28:7901–10.
26. Watanabe K, Ueno M, Kamiya D, Nishiyama A, Matsumura M, Wataya T, et al. A ROCK inhibitor permits survival of dissociated human embryonic stem cells. Nat Biotechnol. 2007; 25:681–6. [PubMed: 17529971]
27. Yao S, Chen S, Clark J, Hao E, Beattie GM, Hayek A, et al. Long-term self-renewal and directed differentiation of human embryonic stem cells in chemically defined conditions. Proc Natl Acad Sci U S A. 2006; 103:6907–12. [PubMed: 16632596]
28. Ross AM, Jiang ZX, Bastmeyer M, Lahann J. Physical aspects of cell culture substrates: topography, roughness, and elasticity. Small. 2012; 8:336–55. [PubMed: 22162324]
29. Baker DE, Harrison NJ, Maltby E, Smith K, Moore HD, Shaw PJ, et al. Adaptation to culture of human embryonic stem cells and oncogenesis in vivo. Nat Biotechnol. 2007; 25:207–15. [PubMed: 17287758]
30. Pyle AD, Lock LF, Donovan PJ. Neurotrophins mediate human embryonic stem cell survival. Nat Biotechnol. 2006; 24:344–50. [PubMed: 16444268]
31. Ejaz M, Yamamoto S, Ohno K, Tsujii Y, Fukuda T. Controlled graft polymerization of methyl methacrylate on silicon substrate by the combined use of the Langmuir-Blodgett and atom transfer radical polymerization techniques. Macromolecules. 1998; 31:5934–6.
32. Huang X, Wirth MJ. Surface initiation of living radical polymerization for growth of tethered chains of low polydispersity. Macromolecules. 1999; 32:1694–6.
33. Tang W, Matyjaszewski K. Kinetic modeling of normal ATRP, normal ATRP with $[Cu\text{-}^{II}]_0$, reverse ATRP and SR&NI ATRP. Macromol Theor Simul. 2008; 17:359–75.
34. Cheng N, Brown AA, Azzaroni O, Huck WTS. Thickness-dependent properties of polyzwitterionic brushes. Macromolecules. 2008; 41:6317–21.
35. Rubinstein M, Dobrynin AV. Associations leading to formation of reversible networks and gels. Curr Opin Colloid In. 1999; 4:83–7.
36. Huang WX, Skanth G, Baker GL, Bruening ML. Surface-initiated thermal radical polymerization on gold. Langmuir. 2001; 17:1731–6.
37. Azzaroni O, Brown AA, Huck WTS. UCST wetting transitions of polyzwitterionic brushes driven by self-association. Angew Chem Int Edit. 2006; 45:1770–4.
38. Hallab NJ, Bundy KJ, OConnor K, Clark R, Moses RL. Cell adhesion to biomaterials: correlations between surface charge, surface roughness, adsorbed protein, and cell morphology. J Long-Term Eff Med. 1995; 5:209–31.

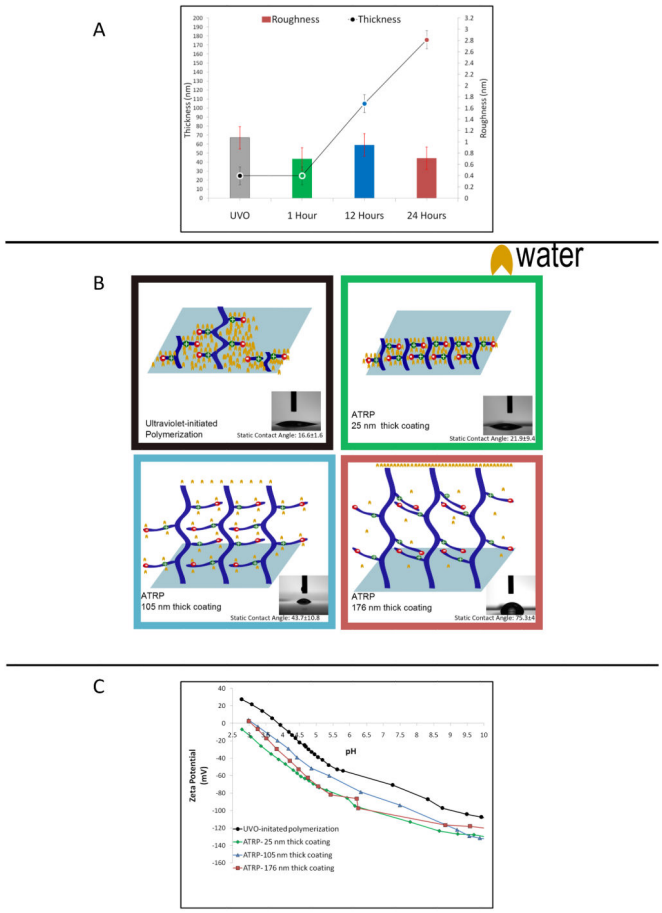

Fig. 1.

Differences in properties of PMEDSAH coatings (A) Thickness (circles) and roughness (columns) of PMEDSAH coatings polymerized through UVO-grafting and ATRP. Thickness of ATRP coatings increased with ATRP reaction time. (1 hour- 25 nm, 12 hours-105 nm, 24 hours- 176 nm) (B) Cartoons depict polymer conformations adopted by the four PMEDSAH coatings studied. Water molecules have been represented in yellow. Differences in hydration and ion-pairing behaviour have been illustrated. Inset- Photographs of static contact angle measurements performed with deionized water on PMEDSAH coatings. Contact angle values are displayed below the respective images. (C) Comparison of zeta potential values of PMEDSAH coatings polymerized through UVO-grafting and ATRP.

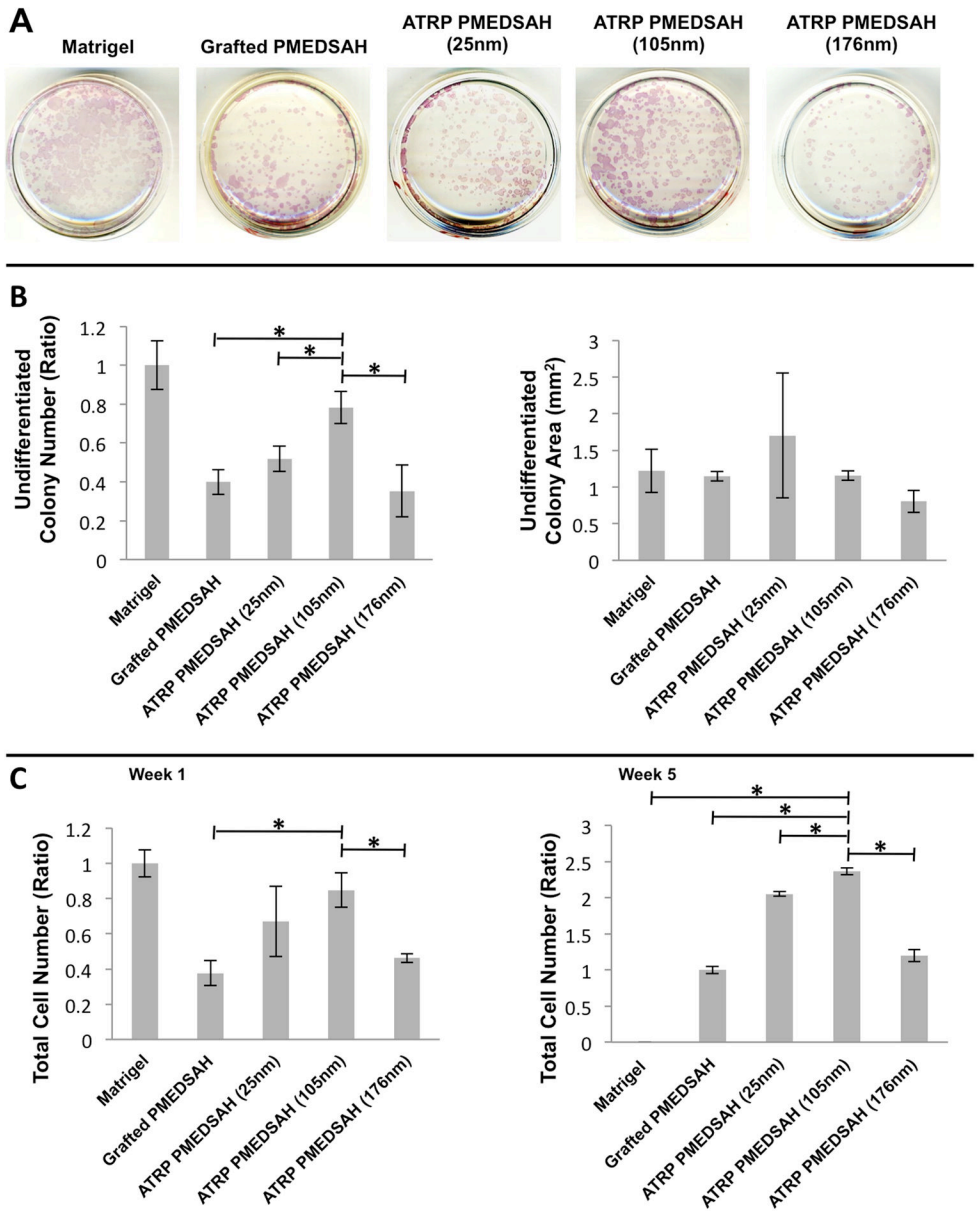

Fig. 2.

Gel architecture influences the undifferentiated colony formation and expansion of hESCs (CHB 10 cells). (A) Undifferentiated colonies were identified by alkaline phosphatase assay after 7 days of culture on different substrates. (B) Plot of undifferentiated colony number ratio compared to Matrigel indicated ATRP PMEDSAH with a 105nm hydrogel thickness lead to a higher number of undifferentiated colonies compared to other experimental groups. Plot of undifferentiated colony area indicated that the areas of undifferentiated colonies cultured on different substrates had no significant differences. (C) Plot of total cell number ratio compared to Matrigel after 1 week and compared to grafted PMEDSAH after 5 weeks indicated ATRP PMEDSAH with a 105nm hydrogel thickness lead to a higher total cell

number compared to other experimental groups. Data in (B) & (C) presented as mean ± standard deviation (SD) from three independent experiments (* $p<0.05$).

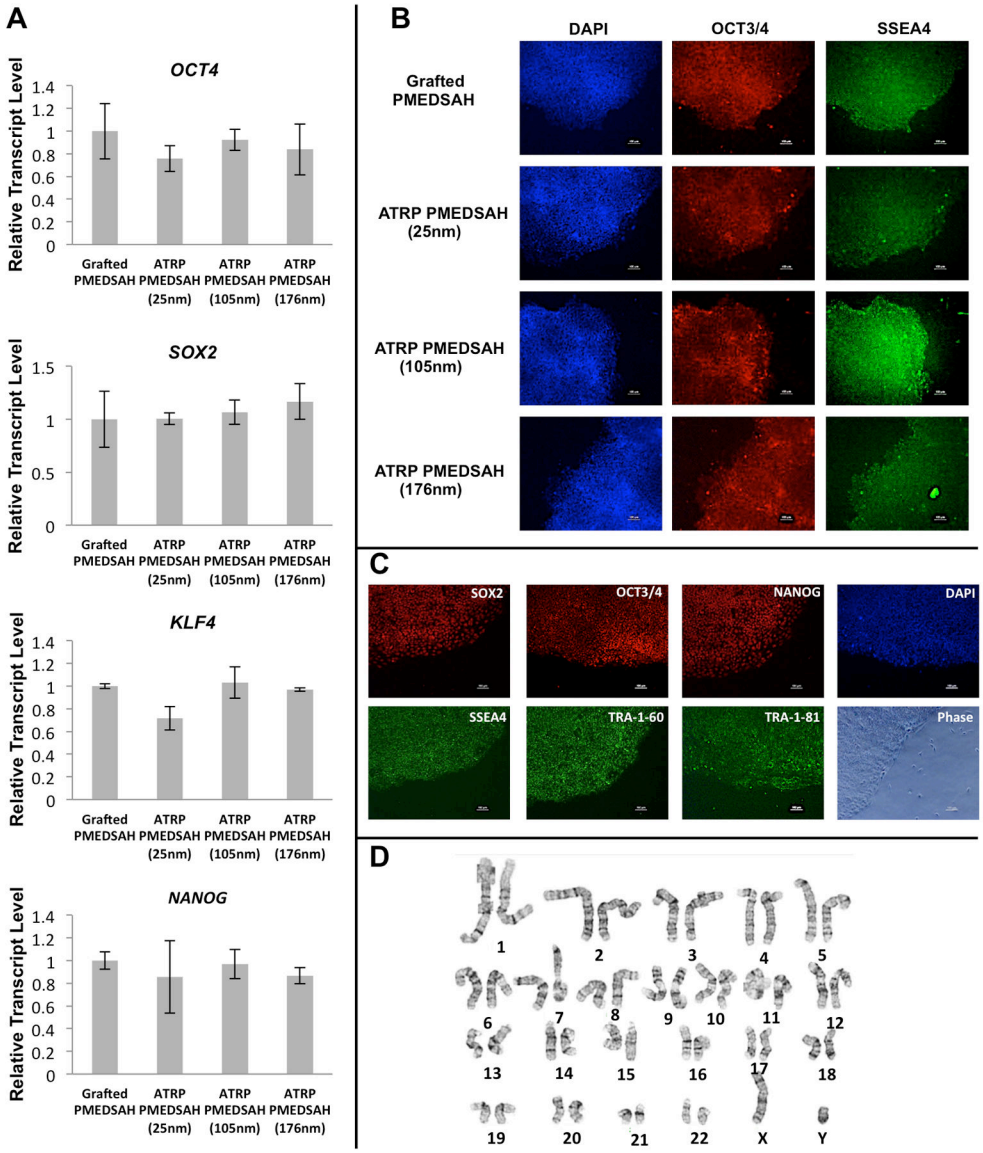

Fig. 3.

Modified PMEDSAH supports hESC stemness and keeps the genomic stability. (A) Relative ranscript levels of OCT4, SOX2, KLF4 and NANOG from hESCs cultured on grafted PMEDSAH and ATRP PMEDSAH after 5 passages had no significant differences. Data presented as mean ± SD from three independent experiments. (B) Fluorescence micrographs of colonies of hESCs cultured on grafted PMEDSAH and ATRP PMEDSAH showing expression of pluripotent markers after 5 passages. Primary antibodies OCT4 and SSEA-4 were used to detect the expression of these markers from hESCs cultured on grafted PMEDSAH and ATRP PMEDSAH (25nm, 105nm and 176nm). hESC cultured on 105nm ATRP PMEDSAH after 5 passages (C) showed expression of pluripotent markers in fluorescence micrographs and (D) kept a normal karyotype.

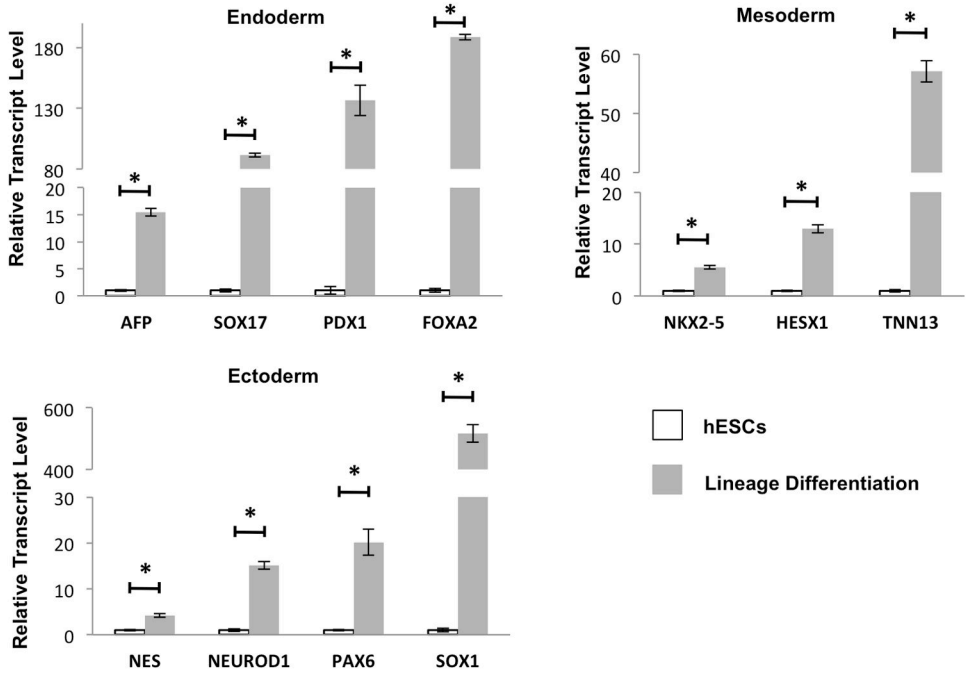

Fig. 4.

Modified PMEDSAH supports hESC pluripotency. hESCs cultured on 105nm ATRP PMEDSAH after 5 passages retained pluripotency as demonstrated by induced specific lineage differentiation with expression of genes representing different germ layers. Data presented in as mean ± SD from three independent experiments.

Table 1

Calculated total cell number of hESCs cultured on different substrates

Substrates	Calculated total cell numbers from Week 0 to Week 5					
	W0	**W1**	**W2**	**W3**	**W4**	**W5**
Matrigel	2×10^4	3.7×10^5	2.4×10^5	3.5×10^6	1.2×10^6	/
Grafted PMEOSAH	2×10^4	1.4×10^5	8.2×10^5	5.0×10^6	2.7×10^7	1.4×10^8
ATRP PMEDSAH (25nm)	2×10^4	2.5×10^5	2.4×10^6	3.4×10^7	2.9×10^8	2.9×10^9
ATRP PMEDSAH (105nm)	2×10^4	3.2×10^5	4.0×10^6	4.9×10^7	4.0×10^8	4.7×10^9
ATRP PMEDSAH (176nm)	2×10^4	1.7×10^5	1.4×10^6	1.0×10^7	6.2×10^7	3.7×10^8

Formula: $CN_{(n+1)} = CN_n \times TN_{(n+1)}/20000$

CN: Calculated total cell number, *TN*: total cell number, *n*: culture week number

Table 2

EB formation with expression of genes representing different germ layers. EBs were formed from hESCs cultured on 105nm ATRP PMEDSAH after 5 passages. Quantitative RT-PCR showed increasing transcript levels of genes representing different germ layers from EBs compared to the undifferentiated hESCs grown on 105 nm ATRP PMEDSAH after 5 passages.

	Gene	Relative Transcript Levels ± SD
Endodrm	*PDX1*	35.58 ± 2.58
	AFP	53.14 ± 4.76
	SOX17	159.47 ± 12.51
	FOXA2	249.12 ± 25.67
Mesoderm	*HESX1*	10.21 ± 0.84
	TNN13	94.32 ± 6.99
	NKX2-5	117.31 ± 4.04
Ectoderm	*NES*	3.58 ± 0.15
	SOX1	37.26 ± 1.35
	PAX6	107.36 ± 7.27
	NEUROD1	860.77 ± 97.08